Supporting Information for

β-FeOOH: A new anode for potassium-ion batteries

Xiaodong Shi [a], Liping Qin[b], Guofu Xu [a,c], Shan Guo [a], Shuci Ma [a], Yunxiang Zhao [a], Jiang Zhou [a,c] *, Shuquan Liang [a,c] *

[a] School of Materials Science and Engineering, Central South University, 932 South Lushan Road, Changsha 410083, Hunan, P.R. China.

[b] College of Biological and Chemical Engineering, Guangxi University of Science and Technology, Liuzhou 545006, Guangxi, P.R. China

[c] Key Laboratory of Electronic Packaging and Advanced Functional Materials of Hunan Province, Central South University, 932 South Lushan Road, Changsha 410083, Hunan, P.R. China

* Corresponding Authors. E-mail address: zhou_jiang@csu.edu.cn; lsq@csu.edu.cn

1. Experimental Section

1.1 Materials and chemicals

Ferric chloride hexahydrate ($FeCl_3 \cdot 6H_2O$), glycerol ($C_3H_8O_6$) and potassium metal were purchased from *Aladdin*. Super P was obtained from *Taiyuan Yingze Force Source Battery Department*. Four kind of electrolytes, i.e. 0.8 M potassium hexafluorophosphate (KPF_6) in ethylene carbonate/diethyl carbonate (EC:DEC, 1:1 in volume), 1 M potassium bis(fluoroslufonyl)imide (KFSI) in EC:DEC, 1 M KFSI in 1,2-dimethoxyethane (DME) and 1 M KPF_6 in DME were obtained from *Suzhou dodochem Ltd*.

1.2 Synthesis of β-FeOOH-SP composite and β-FeOOH

5 mmol $FeCl_3 \cdot 6H_2O$ was dissolved in the mixed solvent of 44 mL deionized water and 6 mL $C_3H_8O_6$. Then, 150 mg Super P was gradually added to the above brown-yellow solution under continuous magnetic agitation. The mixture was keep stirring for 2 h and moving to ultrasonic machine for another 2 h. Afterwards, the black mixtures were transferred to a 60 mL Teflon-lined stainless-steel autoclave and heated at 150 °C for 10 h. Finally, the resultant suspensions were filtered and washed three times with distilled water and ethyl alcohol. After drying at 80 °C in a vacuum oven overnight, the composite of β-FeOOH and Super P were obtained and aliased as FeOOH-SP. As a counterpart, β-FeOOH was prepared through the same method without the addition of Super P.

1.3 Materials characterizations

X-ray diffraction (XRD) pattern of powder samples were characterized by Rigaku 2500 radiation (Cu Kα, λ=0.15405 nm). *In-situ* XRD results of electrode were acquired by Bruker D8 ADVANCE (Cu Kα). Morphology measurements and element analysis were analyzed by Scanning electron microscopy (SEM, NovaNanoSEM230), Energy dispersive X-ray spectroscopy (EDS) and Transmission electron microscope (TEM, HEM-2100F/UHR). Thermogravimetric analysis (TGA) was investigated on simultaneous thermal analyzer (Netzsch STA449C). X-ray photoelectron spectra (XPS) was performed on an ESCALAB 250Xi spectrometer. Nitrogen isothermal adsorption desorption data were tested on multi-station adsorption apparatus (Micromeritics ASAP 2460).

1.4 Electrochemical test of PIBs

The electrodes were prepared by coating a mixed slurry composed of FeOOH-SP

composite (85 wt.%), Super P (5 wt.%) and sodium alginate (10 wt.%) on copper foil, and drying at 80 °C for 12 h in a vacuum oven. The working electrode was cut into small pieces with a diameter of 12 mm. The mass loading of active material on Cu foil is about ~1.2 mg cm^{-2}. Subsequently, these electrodes were coupled with potassium foil, electrolytes and glass fibers membrane, and assembled in glove box filled with high purity argon. The electrolytes used in this work were 0.8 M KPF_6 in EC:DEC, 1 M KFSI in EC:DEC, 1 M KPF_6 in DME and 1 M KFSI in DME. Meanwhile, all the capacities and current densities in this work were normalized by the mass of FeOOH-SP composite unless otherwise stated.

Galvanostatic charge/discharge profiles, cyclic performances and rate capabilities were conducted on LAND CT2001 test system (*Wuhan LAND Electronic Co. Ltd*) at different current densities at room temperature. Cyclic voltammetry plots were tested on a CHI660E electrochemical workstation (*Shanghai Chenhua Instrument Co. LTD*) at different scan rates, in which electrochemical impedance spectroscopy was also carried out within the frequency range from 10 mHz to 100 kHz.

2. Related calculation formulas

2.1 Calculation of capacitive contribution ratio

At a certain potential, the response current can be divided into two components according to the Formula S1, by introducing two parameters, i.e. k_1 and k_2.

$$i = k_1 v + k_2 v^{1/2} \qquad \text{(S1)}$$

$$i/v^{1/2} = k_1 v^{1/2} + k_2 \qquad \text{(S2)}$$

$k_1 v$ originates from the capacitive contribution, $k_2 v^{1/2}$ originates from the diffusion-limited Faradaic processes. By processing the above Formulas into the following format (Formula S2), we can separate these two processes based on the linear relationship between $i/v^{1/2}$ and $v^{1/2}$.

2.2 Calculation of diffusion coefficient based on GITT

The diffusion coefficient based on the galvanostatic intermittent titration technique (GITT) could be calculated by Formula S3.

$$D = \frac{4}{\pi t}\left(\frac{mV}{MS}\right)^2\left(\frac{\Delta E_s}{\Delta E_t}\right)^2 \qquad \text{(S3)}$$

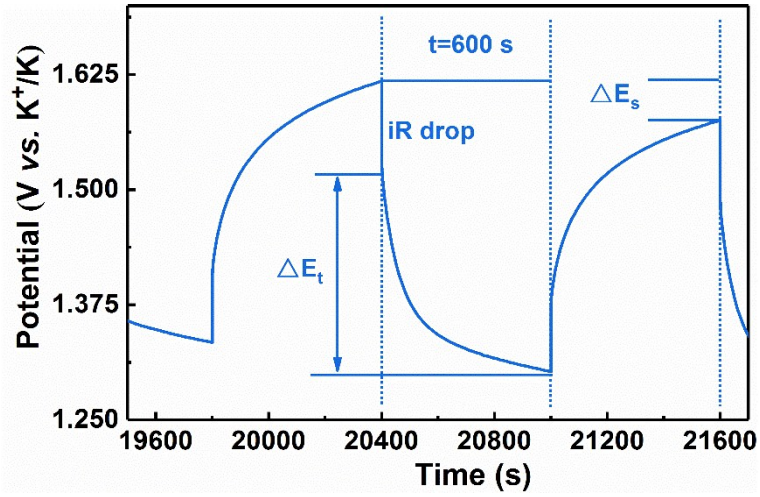

t is the duration time of current pulse, m is the mass load of active material on the electrode, S is the area of electrode, ΔE_s is the quasi-thermodynamic equilibrium potential difference before and after the current pulse, ΔE_t is the potential difference during current pulse, V and M is the molar volume and molar mass of active material.

2.3 Calculation of *b* value

The response current in the CV obeys the relationship of Formula S4 and S5.

$$i = a\, v^b \quad \text{(S4)}$$

$$\log(i) = \log a + b \log(v) \quad \text{(S5)}$$

2.4 Calculation of diffusion coefficient based on EIS

Based on Formula S6 and S7, the corresponding slopes (σ) could be obtained through fitting Z'' with $\omega^{-1/2}$. In Formula S8, R: gas constant (8.314 J (mol K)$^{-1}$), T: Kelvin temperature (298 K), S: area of working electrode (1.13 cm^2), n: electronic transfer number, F: Faraday constant (96485 C mol^{-1}) and C: concentration of K^+ ions in the lattice (i.e. concentration of electrolyte).

$$\omega = 2\pi f \quad \text{(S6)}$$

$$Z'' = R + \sigma\omega^{-1/2} \quad \text{(S7)}$$

$$D = 0.5R^2T^2/S^2n^4F^4C^2\sigma^2 \quad \text{(S8)}$$

3. Supplementary Figures

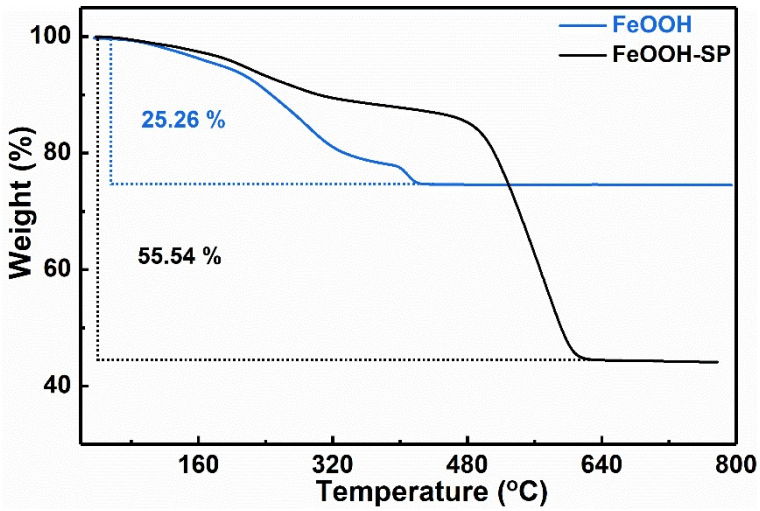

Figure S1 TGA curves of (a) β-FeOOH and (b) FeOOH-SP composite.

In order to calculate the mass loading of β-FeOOH in FeOOH-SP composite, the thermogravimetric analysis (TGA) curves of bare β-FeOOH and FeOOH-SP composite have been investigated. As shown in Fig. S1, the weight loss of β-FeOOH and FeOOH-SP composite are 25.26 % and 55.54 %, respectively. The weight decrease of FeOOH-SP composite could be illustrated as the following Formulas, in which *C* represents the weight of FeOOH-SP composite and *x* represents the content of β-FeOOH in FeOOH-SP composite.

$$C*55.54\%=C*x*25.26\%+C*(1-x)$$

Therefore, *x* is calculated as 59.49 %. *i.e.* the mass content of β-FeOOH in FeOOH-SP composite is 59.49 %, while the content of Super P is 40.51 %.

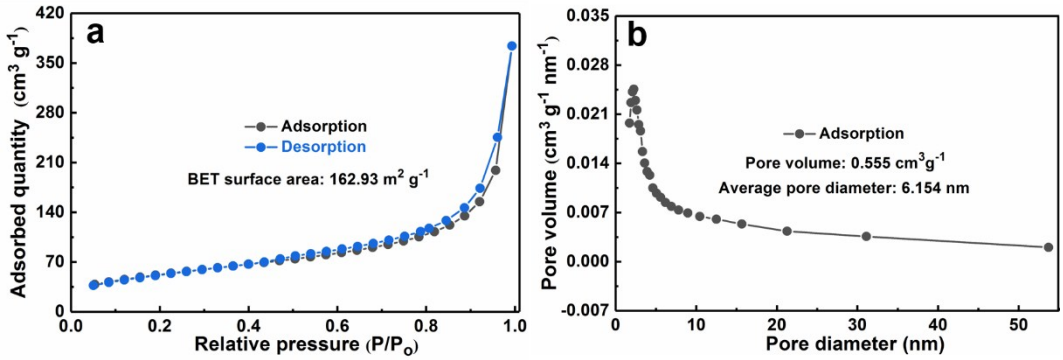

Figure S2 (a) Nitrogen isothermal adsorption desorption curves and (b) pore size distribution of FeOOH-SP composite

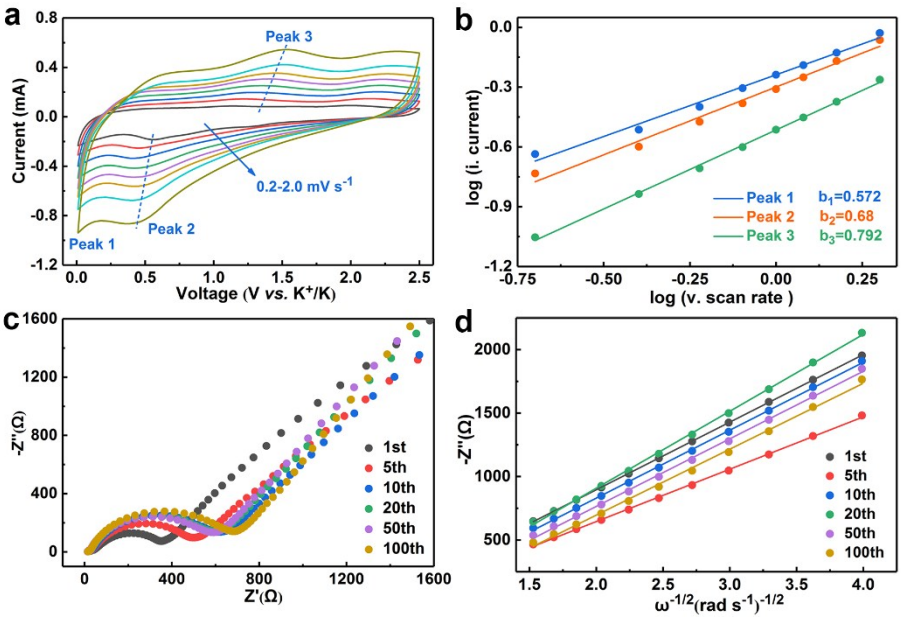

Figure S3 (a) CV curves of FeOOH-SP electrode at different scan rates range from 0.2 mV s^{-1} to 2.0 mV s^{-1}; (b) log (*i*) *vs.* log (*v*) plots of FeOOH-SP electrode at certain peak currents; (c) Electrochemical impedance spectroscopy and (d) Warburg factors of FeOOH-SP electrode after different cycles.

As shown in Fig. S3a, CV curves at different scan rate (0.2-2.0 mV s^{-1}) have been collected to disclose the potassium storage kinetics of FeOOH-SP electrode. With the increase of scan rates, the redox peaks in CV curves could be well maintained, in which the peak currents comply with the relationship of Formula S4, and *b* value could be calculated through Formula S5. Detailedly, based on the results in Fig. S3b, *b* values corresponding to two reduction peaks (0.55 V and 0.01 V) are 0.572 and 0.68, respectively, suggesting that the potassiation reaction of FeOOH-SP electrode is controlled by K^+ ions diffusion reaction.

To confirm the structure stability, EIS and relevant Warburg factors (σ) of FeOOH-SP electrode after different cycles have been investigated and presented in Fig. S3c-S3d, in which charge transfer resistance (R_{ct}) turns larger with the increase of cycle numbers due to the accumulation of irreversible products during cycling process. Additionally, according to Formulas S6-S8, Warburg factor (σ) could be calculated through the linear slope of Z'' with $\omega^{-1/2}$ and it could be detected that σ value has no significant change with the increase of cycle numbers, demonstrating the stable K^+ ions diffusion behavior.

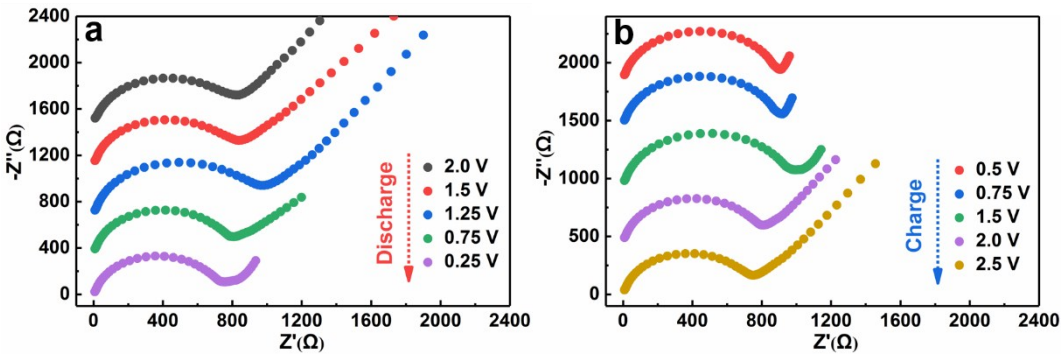

Figure S4 Electrochemical impedance spectroscopy (EIS) of FeOOH-SP electrode in different (a) discharge voltages and (b) charge voltages during the first (de)potassiation process.

Ex-situ EIS of FeOOH-SP electrode have been supplemented to analyze the changes of charge transfer impedance (R_{ct}) during the first (de)potassiation process. As shown in Fig. S4a, the value of R_{ct} gradually increases with the discharge voltage up to 1.25 V. As demonstrated by *in-situ* XRD (Fig. 4a-4b), the β-FeOOH changes from crystalline to amorphous structure when discharged to 1.26 V, accompany with the increase of charge transfer impedance. [1] When increasing the discharge depth from 1.25 to 0.25 V, the value of R_{ct} gradually decreases due to the continuous insertion of K^+ ions. [2, 3]

On the contrary, the value of R_{ct} gradually increases with the increase of charge depth up to 1.5 V (Fig. S4b) owing to the extraction of K^+ ions. Subsequently, the decrease of charge transfer impedance from 1.5 to 2.5 V could be attributed to the partial regeneration of crystalline structure. [4]

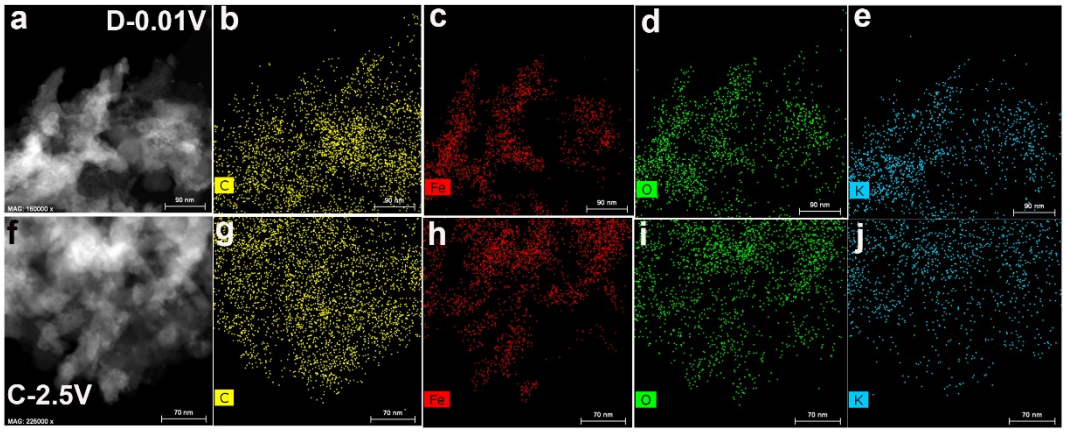

Figure S5 Element mapping images of FeOOH-SP electrode at (a-e) fully discharged state and (f-j) fully charged state.

Table S1 Calculation of the capacity contribution of SP and FeOOH in FeOOH-SP at 100 mA g^{-1} in different cycles.

Cycle number at100 mA g^{-1}	40th	60th	80th	100th
Reversible capacity of FeOOH-SP (mA h g^{-1})	179.8	181.7	187.6	178.1
Reversible capacity of SP (mA h g^{-1})	93.9	89.7	89	86.4
Capacity contribution of SP to FeOOH-SP (mA h g^{-1})	38.04	36.34	36.05	35
Capacity contribution of FeOOH to FeOOH-SP (mA h g^{-1})	141.76	145.36	151.55	143.1
Capacity contribution ratio of SP	**21.15 %**	**20 %**	**19.2 %**	**19.65 %**
Capacity contribution ratio of FeOOH nanocrystals	78.85 %	80 %	80.8 %	80.35 %

The capacity contribution of SP to FeOOH-SP is equal to the SP content (40.51 wt.%, **Fig. S1**) in FeOOH-SP multiplied by the reversible capacity of SP (**Fig. 2d**). The contribution of FeOOH to FeOOH-SP is equal to the reversible capacity of FeOOH-SP minus the capacity contribution of SP. The capacity contribution ratio of SP is equal to the capacity contribution of SP divided by the reversible capacity of FeOOH-SP. The capacity contribution ratio of FeOOH is equal to the capacity contribution of FeOOH divided by the reversible capacity of FeOOH-SP.

As a result, the high capacity of FeOOH-SP is majorly attributed to the FeOOH component.

References:

1. G. Fang, Z. Wu, J. Zhou, C. Zhu, X. Cao, T. Lin, Y. Chen, C. Wang, A. Pan and S. Liang, *Adv. Energy Mater.*, 2018, **8**, 1703155.

2. P. Ge, H. Hou, S. Li, L. Yang and X. Ji, *Adv. Funct. Mater.*, 2018, **28**, 1801765.

3. G. Zhao, Y. Zhang, L. Yang, Y. Jiang, Y. Zhang, W. Hong, Y. Tian, H. Zhao, J. Hu, L. Zhou, H. Hou, X. Ji and L. Mai, *Adv. Funct. Mater.*, 2018, **28**, 1803690.

4. H. Hou, C. E. Banks, M. Jing, Y. Zhang and X. Ji, *Adv. Mater.*, 2015, **27**, 7861-7866.